PAPER • **OPEN ACCESS**

Electrodeposited WS_2 monolayers on patterned graphene

To cite this article: Y J Noori *et al* 2022 *2D Mater.* **9** 015025

View the article online for updates and enhancements.

You may also like

- Effects of data quality vetoes on a search for compact binary coalescences in Advanced LIGO's first observing run
B P Abbott, R Abbott, T D Abbott et al.
- IPEM topical report: the first UK survey of dose indices from radiotherapy treatment planning computed tomography scans for adult patients
Tim J Wood, Anne T Davis, James Earley et al.
- Black holes, gravitational waves and fundamental physics: a roadmap
Abbas Askar, Chris Belczynski, Gianfranco Bertone et al.

This content was downloaded from IP address 152.78.0.24 on 10/01/2022 at 11:46

2D Materials

PAPER

Electrodeposited WS_2 monolayers on patterned graphene

Y J Noori[1,5,*], S Thomas[2], S Ramadan[3], V K Greenacre[2], N M Abdelazim[1], Y Han[4], J Zhang[1], R Beanland[4], A L Hector[2], N Klein[3], G Reid[2], P N Bartlett[2] and C H de Groot[1,*]

[1] School of Electronics and Computer Science, University of Southampton, Southampton SO17 1BJ, United Kingdom
[2] School of Chemistry, University of Southampton, Southampton SO17 1BJ, United Kingdom
[3] Department of Materials, Imperial College, London SW7 2AZ, United Kingdom
[4] Department of Physics, University of Warwick, Coventry CV4 7AL, United Kingdom
[5] Optoelectronics Research Centre, University of Southampton, Southampton SO17 1BJ, United Kingdom
[*] Authors to whom any correspondence should be addressed.

E-mail: y.j.noori@southampton.ac.uk **and** chdg@southampton.ac.uk

Keywords: electrodeposition, 2D materials, , TMDC, tungsten disulfide, WS_2, graphene, heterostructure

Supplementary material for this article is available online

OPEN ACCESS

RECEIVED
6 October 2021

REVISED
19 November 2021

ACCEPTED FOR PUBLICATION
26 November 2021

PUBLISHED
10 December 2021

Original content from this work may be used under the terms of the Creative Commons Attribution 4.0 licence.

Any further distribution of this work must maintain attribution to the author(s) and the title of the work, journal citation and DOI.

Abstract

The development of scalable techniques to make two-dimensional (2D) material heterostructures is a major obstacle that needs to be overcome before these materials can be implemented in device technologies. Electrodeposition is an industrially compatible deposition technique that offers unique advantages in scaling 2D heterostructures. In this work, we demonstrate the electrodeposition of atomic layers of WS_2 over graphene electrodes using a single source precursor. Using conventional microfabrication techniques, graphene was patterned to create micro-electrodes where WS_2 was site-selectively deposited to form 2D heterostructures. We used various characterization techniques, including atomic force microscopy, transmission electron microscopy, Raman spectroscopy and x-ray photoelectron spectroscopy to show that our electrodeposited WS_2 layers are highly uniform and can be grown over graphene at a controllable deposition rate. This technique to selectively deposit transition metal dichalcogenides over microfabricated graphene electrodes paves the way towards wafer-scale production of 2D material heterostructures for nanodevice applications.

1. Introduction

The exceptional optoelectronic properties of two-dimensional (2D) transition metal dichalcogenides (TMDCs) have made these materials a hot research topic since the early 2010s. Among the TMDC family, tungsten disulfide (WS_2) stands out for its high quantum yield which makes it exhibit strong photoluminescence, as well as its high electrical performance and ambipolar field effect behavior [1–9]. Emerging technological applications of tungsten disulfide include bright light emitting devices, high responsivity photodetectors, sensitive gas sensors and optical identification labels [10–12]. Heterostructures comprising of several 2D materials can harness the unique properties of their individual material constituents to make new device technologies that have the potential to surpass the performances of those commercialized and reported in the literature. For example, several papers have demonstrated photodetection by combining the unique semiconductor properties of WS_2 with that of graphene, offering photodetectors with broadband detection capability and high photoresponsivity [13–16].

The challenges associated with scaling the production of 2D material heterostructures present a major obstacle that hinders their adoption in industry. There are several scalable techniques that have been used to deposit WS_2, such as chemical vapor deposition (CVD), atomic layer deposition, plasma sputtering, pulsed laser deposition, thermal decomposition, liquid exfoliation and electrodeposition [7, 16–22]. Among these, CVD stands out because it can controllably deposit monolayer of various TMDC materials with very high crystallinity. Kim *et al* showed the potential of this technique in achieving large scale production of TMDCs [23]. However, CVD grown 2D materials and their heterostructures require layer transfer for most device integration [24, 25]. CVD also typically require elevating the

© 2021 The Author(s). Published by IOP Publishing Ltd

host substrates to temperatures that exceed 800 °C, which damage 2D materials such as graphene existing on the substrate [26]. These issues also limit the practicality of CVD in fabricating large numbers of 2D material heterostructure devices on each chip. Khadka *et al* used CVD to demonstrate selective growth of high quality TMDCs on transition metal films [27]. Plasma based deposition techniques are also known to cause ion bombardment of the substrate, which causes crystal defects on other materials such as graphene [28, 29].

In comparison, electrodeposition is a room temperature technique that lends itself to depositing materials selectively over conductive electrodes. It is used routinely in the semiconductor industry such as in depositing magnetic films for hard drive read/write heads, or in creating Cu chip interconnects, using the damascene process [30, 31]. We have previously used electrodeposition to grow few-layer MoS_2 films [32, 33]. A few works have demonstrated the electrodeposition of bulk WS_2 thin films over traditional electrodes such as platinum and indium tin oxide using aqueous and acetonitrile solutions [34–36]. $[NH_4]_2[WS_4]$ was commonly used as the precursor in these studies, however, it resulted in S-rich thin films and has not shown yet to deposit smooth ultrathin films of WS_2. In our recent work, we have shown that WS_2 thin films can be electrodeposited using dichloromethane (CH_2Cl_2), over TiN electrodes [22]. Electrodepositing from CH_2Cl_2 and avoiding the need for addition of a proton source (that is necessary to remove the excess S when using $[WS_4]^{2-}$ as the precursor) increases the faradaic efficiency and extends the accessible potential window for depositing a variety of technologically important materials that may not otherwise be possible using aqueous or acetonitrile electrolytes [37, 38]. CH_2Cl_2 is also relatively inert, less viscous than ionic liquids and is only weakly coordinating. We have performed our deposition using a single source precursor based on $[NEt_4]_2[WS_2Cl_4]$. Compared to $[NH_4]_2[WS_4]$, the advantage of this precursor is that it can be dissolved readily in CH_2Cl_2 and contains the correct W:S ratio for WS_2, so there is no excess S to be removed.

Challenges associated with graphene production at wafer scales have already been solved using CVD and the wet transfer technique. Several groups have demonstrated wafer-size graphene and several spin-out companies have recently emerged to exploit the commercial opportunities from this advancement, such as Graphenea Inc. and Grolltex Inc. [39–41]. By fabricating graphene micro-electrodes at wafer scales, one can use the scalability advantages offered by electrodeposition to site-selectively deposit a variety of TMDCs to form 2D material heterostructures for device applications.

There are two aspects to the novelty of this work. Firstly, it represents the first electrochemical deposition of atomically thin WS_2 films over graphene electrodes. Most importantly, the deposited films presented here show far superior material uniformity and continuity compared to other electrodeposited WS_2 films from previous reports [34–36]. Secondly, we have shown that we can make microscale WS_2/graphene heterostructures by patterning the graphene electrodes using conventional microfabrication techniques. This represents a major step towards scaling the production of 2D materials and their heterostructures into wafer sizes via electroplating. Throughout the work we present results from characterizing the electrodeposited WS_2 using various techniques including atomic force microscopy (AFM), transmission electron microscopy (TEM), Raman spectroscopy and x-ray photoelectron spectroscopy (XPS).

2. Experimental

2.1. Electrode microfabrication

The graphene films used in this work were prepared by CVD on Cu foils and transferred to the Si/SiO_2 substrates through the wet transfer method. Details of this process have been reported previously [42, 43]. A chrome/gold pad was deposited over part of the graphene film to reduce the contact resistance between the graphene and the contact to the potentiostat.

Monolayer graphene micro-electrodes were fabricated using conventional microfabrication techniques. A photoresist was spin-coated on the graphene over an Si/SiO_2 substrate. The pattern was transferred to the graphene film via UV lithography and reactive ion etching (RIE) using the photoresist as an etching mask. Graphene RIE etching was performed in an O_2 plasma for 90 s. While shorter etching periods can be used to pattern the monolayer graphene electrodes, over etching was done to ensure that all exposed graphene or residues of photoresists are removed completely. The photoresist was then removed to expose the protected graphene micro-electrodes. Figure 1(a) shows the layout of the photolithography mask used in this work. The resultant graphene electrodes are presented in figures 1(b) and (c). The smallest feature of the fabricated electrodes was approximately 9 μm. A Raman map of the graphene micro-electrodes was recorded by scanning through part of the electrodes and plotting the intensity of the graphene 2D peak (2691 cm^{-1}) as shown in the inset of figure 1(c). A typical Raman spectrum recorded from graphene electrodes is shown in figure S1 in the supporting information (available online at stacks.iop.org/2DM/9/015025/mmedia). Based on the 2D/G Raman intensity ratio, and the optical microscope images, it is evident that the graphene electrode is a monolayer [44–48]. The Raman spectrum shows that the quality of the graphene remains high after the fabrication process. AFM images

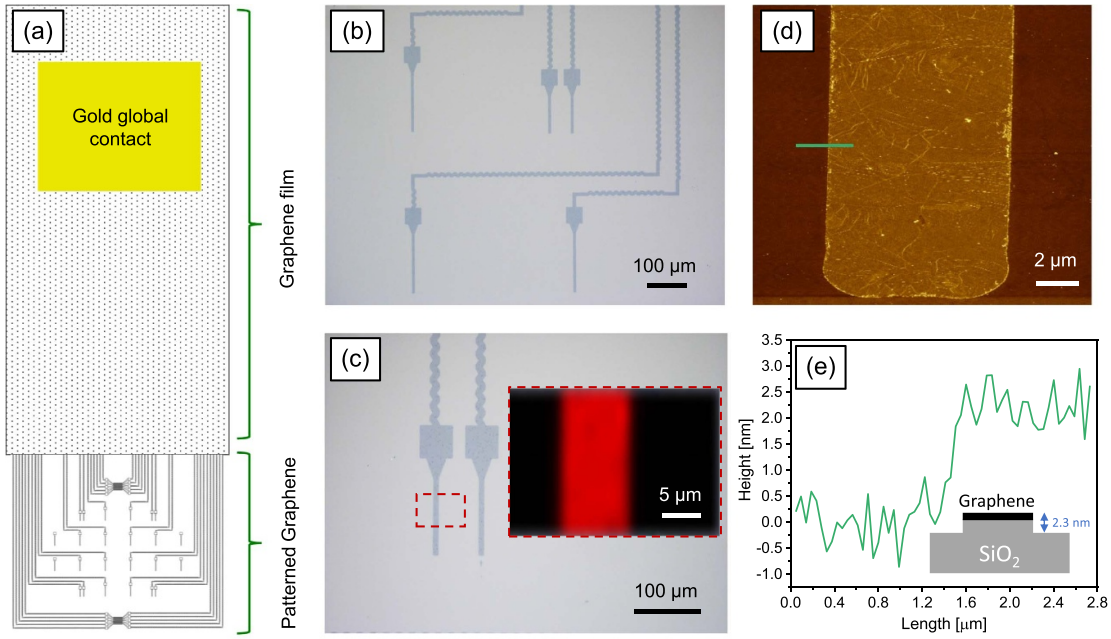

Figure 1. (a) Schematic diagram of the photolithography mask that was used in patterning the graphene electrodes. (b) Optical microscope image showing the graphene electrodes after fabrication. (c) Optical microscope image showing the graphene electrodes at higher magnification with a Raman map (inset) of the bare graphene. (d) AFM image of a graphene electrode after fabrication and a step height profile (e) taken at the edge of the electrode.

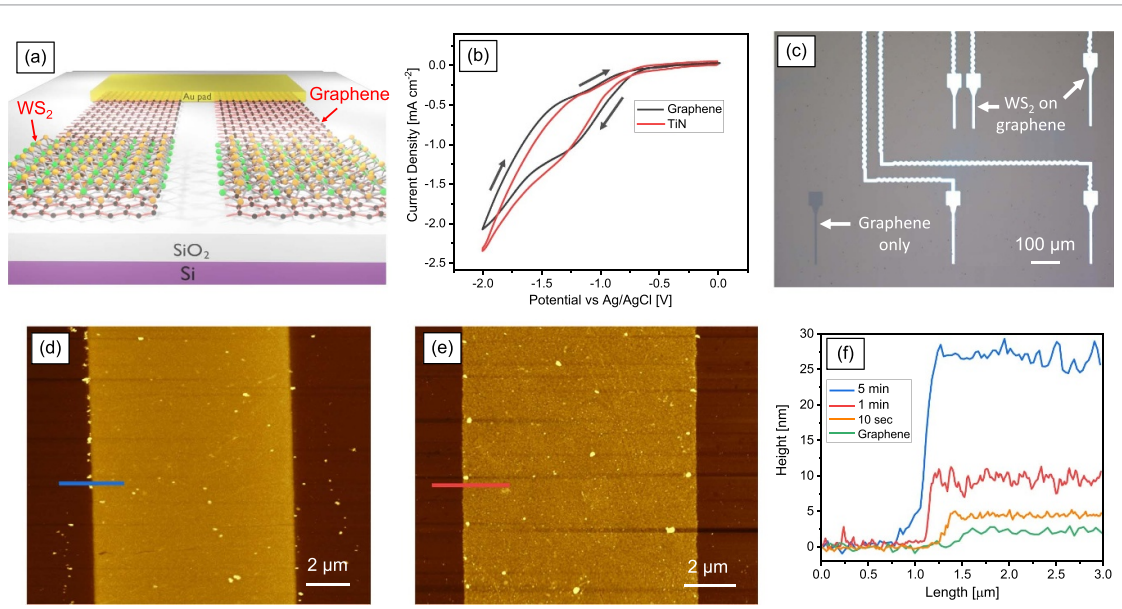

Figure 2. (a) A schematic illustration of the concept of this work showing WS_2 2D materials deposited on patterned graphene stripes that are biased through an Au contact pad. (b) Cyclic voltammetry scans of the $[NEt_4]_2[WS_2Cl_4]$ precursor in DCM taken using graphene and TiN electrodes. (c) An optical microscope image showing the contrast difference between a patterned WS_2/graphene heterostructure and bare graphene film. AFM topography images of WS_2 deposits on graphene for 5 min (d) and 1 min (e). (f) Line profiles taken at the edges of the deposited films showing the total measured step heights.

of the graphene micro-electrodes are presented in figures 1(d)–(e) and figure S2. AFM height analysis of the graphene electrodes shows that the electrodes are on average ∼2.3 nm thick. While this thickness might appear higher than that expected for monolayer graphene, this is due to the relatively long (90 s) RIE etching used, which also resulted in small amount of SiO_2 being physically etched in the oxygen plasma at roughly 1–2 nm min^{-1}, creating a SiO_2 step lower than graphene, see inset in figure 1(e).

2.2. Electrodeposition of WS_2

Figure 2(a) illustrates the concept of this work showing WS_2 2D material over fabricated graphene strips. The graphene is connected to a large Au pad through which an electrochemical potential is applied. All

the electrodeposition experiments, including the electrolyte preparation were carried out inside a glovebox equipped with a nitrogen recirculation system to maintain its O_2 and H_2O levels below 10 ppm. The electrodeposition processes were performed using a three-electrode electrochemical cell that comprises a Pt/Ir (90:10 elemental composition) disc as the counter electrode and a reference electrode made of an Ag/AgCl wire placed within a glass frit containing 0.1 M $[N^nBu_4]Cl$ in CH_2Cl_2. The single source precursor, $[NEt_4]_2[WS_2Cl_4]$, was dissolved in CH_2Cl_2 containing 0.1 M containing $[N^nBu_4]Cl$. Details of the synthesis of this precursor has been reported previously [49]. Prior to the experiment, the CH_2Cl_2 was dried and degassed by distillation from CaH_2 to minimize its water content. The H_2O content was measured by Karl-Fischer titration to be ca. 18 ppm.

The electrochemical behavior of the precursor in CH_2Cl_2 was studied by performing cyclic voltammetry as shown in figure 2(b). The graphene and TiN electrodes chosen for the CV experiments were circularly shaped with a 4 mm diameter to ensure that a good electrical signal is obtained for the CV comparison. The potential was swept twice from 0 V to −2 V and back to 0 V as indicated by the arrows. The observed current range was found to be similar for both electrodes indicating that graphene has very similar iR drop to a common conductive material like TiN. The electrochemical behavior of $[NEt_4]_2[WS_2Cl_4]$ on graphene electrode was found to be similar to that on TiN, characterized by a cathodic peak shoulder at around −1.5 V [22]. Based on the electrochemical quartz crystal microbalance studies reported in our previous work, the cathodic deposition of WS_2 (on Pt) starts from −1.2 V and continues in the whole cathodic potential range till −2.0 V.

The WS_2 deposition on graphene microelectrodes was performed by fixing the potential at −1.7 V and changing the deposition time to achieve the desired thickness. The first deposition was performed for a 5 min period. Following the deposition, the substrate was rinsed in pure CH_2Cl_2. Figure 2(c) shows an image of the deposited WS_2 films over the graphene electrodes depicted by bright patterns of zigzag and straight lines as per the mask design. In comparison, a graphene film that has not been connected to the gold pad appear in its original gray color as shown in figure 1, confirming there is no WS_2 deposition on these regions of the graphene film nor the presence of residues from the electrolyte. The as-deposited WS_2 film is amorphous, as shown by the absence of a Raman signal from these films. Therefore, an annealing step was performed to crystallize the film. The electrodeposited film was annealed in a tube furnace at 500 °C for 2 h at 0.1 mbar. The sample was annealed in the presence of sulfur powder in the tube furnace to compensate for the loss of (volatile) sulfur from the film during the process. Thermal annealing was found to significantly improve the crystallinity of the material as shown in the Raman results below.

3. Results and Discussions

3.1. AFM

AFM was used to characterize the thickness of the WS_2/graphene heterostructure and study the uniformity and continuity of the deposited films. Figures 2(d) and (e) show images of two different films grown for 5 and 1 min, respectively. The 5 min deposition shows a total step height thickness of 27.3 nm, while the 1 min deposit shows a step height thickness of 9.5 nm, see figure 2(f). These values correspond to the sum of the step height created in SiO_2 due to over etching, the thickness of the graphene electrode, and the thickness of the deposited WS_2 film. Supporting figure S3 shows more AFM data taken from the 5 min and 1 min films along patterned zigzag lines.

Aiming towards monolayer WS_2, we further reduced the deposition time to 10 s, which led to a step height of 4.4 nm, as illustrated in figures S4 and 2(f). Since the step height before the deposition was measured to be 2.3 nm, the actual thicknesses of the deposited WS_2 for 5 min, 1 min and 10 s are 25 nm, 7.2 nm and 2.1 nm, respectively. The layer-to-layer spacing in WS_2 has been measured before to be approximately 0.65 nm [7, 20]. Hence the 10 s deposit is estimated to have produced a maximum of trilayer WS_2 thickness. The root mean square (RMS) roughness of the 10 s deposit is 0.28 nm. By plotting a graph of the measured thickness vs deposition time, the electrodeposition of WS_2 was found to behave linearly with a deposition rate of 0.10 ± 0.03 nm s^{-1}, see supporting figure S5. The AFM images of the heterostructures show that the electrodeposited films have very good uniformity and continuity across the patterns. The uniformity remains high even for ultra-thin films, including the 10 s deposits. Compared to previous reports of electrodeposited WS_2 that mostly show very rough and discontinuous films, this work represents an important advancement in WS_2 production via electrodeposition, making it a competitive alternative deposition technique [34–36]. It is also worth noting that each of these depositions was performed using solutions prepared on different days, using different batches of synthesized precursor, indicating good repeatability for this process.

3.2. Raman and energy dispersive x-ray (EDX) spectroscopy

Raman spectroscopy is a common technique for characterizing the physical properties of 2D materials and TMDCs. In this work, the presence of WS_2 on the substrate, its uniformity and degree of crystallinity were investigated by measuring the Raman scattering of a 532 nm wavelength laser at room temperature. Light excitation and collection were done via

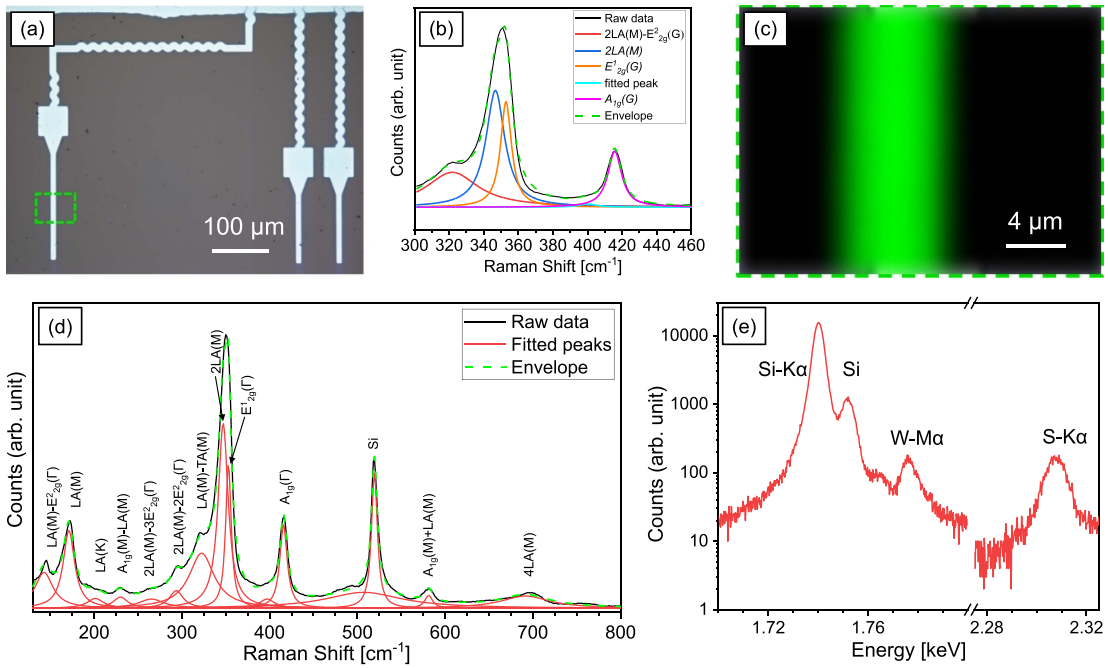

Figure 3. (a) An optical microscope image of patterned WS_2/graphene heterostructure. (b) A typical Raman spectrum taken from the WS_2 deposits showing the signature of the material and the fitted peaks associated with various vibrational modes in the material. (c) A Raman spatial map from the green squared region shown in (a) plotted as function of the intensity of the peak that is composed of the 2LA(M) and E^1_{2g} peaks. (d) A wider Raman spectrum along with the fitted peaks showing the common vibrational modes for WS_2 and Si for the range 100–800 cm^{-1}. (e) A WDX spectrum of deposited WS_2 showing the Mα and Kα energy signatures of W and S, respectively.

a 50× objective lens which can reduce the laser spot diameter to 1 μm to probe the patterned areas.

The consequence of using an excitation wavelength of 532 nm is that the Raman spectrum becomes enriched with second order harmonic modes [50]. Figure 3(a) shows an optical microscope image of patterned WS_2/graphene heterostructures and a dashed line region where Raman spectra and maps were recorded. Figure 3(b) presents a typical spectrum obtained from electrodeposited WS_2 over graphene microelectrodes. Variations in the intensity were observed depending on the thickness of the deposited material. Multi-peak Lorentzian fitting was applied to deconvolute the various peaks from the spectrum. The Raman shift of the E^1_{2g} (Γ) peak, which relates to the in-plane vibration of W and S atoms is at 352.9 cm^{-1}, while the Raman shift of the A_{1g} peak which involves the out-of-plane displacement of S atoms is 415.8 cm^{-1}. The shift difference between the E^1_{2g} and the A_{1g} peaks is 62.9 cm^{-1} and the intensity ratio between the 2LA(M) and the A_{1g} peaks (2LA(M)/A_{1g}) was calculated to be 1.94. A Raman map was recorded by scanning the region at 1 μm steps as shown in figure 3(c). The map is plotted by taking the spatial intensity of the raw signal peak at 350 cm^{-1}. It is clear to see that the map intensity is uniform across the patterned film which indicates that the quality of the film is highly uniform. A wider Raman spectrum of the WS_2 deposit is presented in figure 3(d) showing the presence of all the previously reported peaks from WS_2 with sharpness that is similar to WS_2 grown by CVD or via WO_3 sulfurization, indicating the high quality of the material [50, 51].

A common technique to quantify the composition of a material is to use EDX spectroscopy system attached to an SEM. However, due to the close spectral energy between the Si-Kα and W-Mα electron energy peaks wavelength dispersive x-ray (WDX) spectroscopy was employed instead because it offers much higher spectral resolution to resolve very close energy peaks. Figure 3(e) shows a WDX spectrum obtained from a film deposited for 5 min which had a thickness of roughly 27 nm. We used a relatively thick film, as few-layer films offer poor x-ray signal to noise ratio, making the composition quantification unreliable. The electron energy peaks of W Mα and S Kα peaks were found at 1.776 eV and 2.307 eV, respectively. Fitting analysis of the data was performed using Thermo Scientific NSS spectral imaging software, which showed that the S/W composition ratio was quantified to be 2.0 $\pm$ 0.1. To ensure accurate composition quantification, the WDX values obtained from electrodeposited films are compared to those from commercial single crystals of WS_2 grown by chemical vapor transport as reference.

3.3. TEM

To provide further insight on the physical nature of the film, TEM imaging was performed by taking a lamella slice of the patterned film using a focused ion

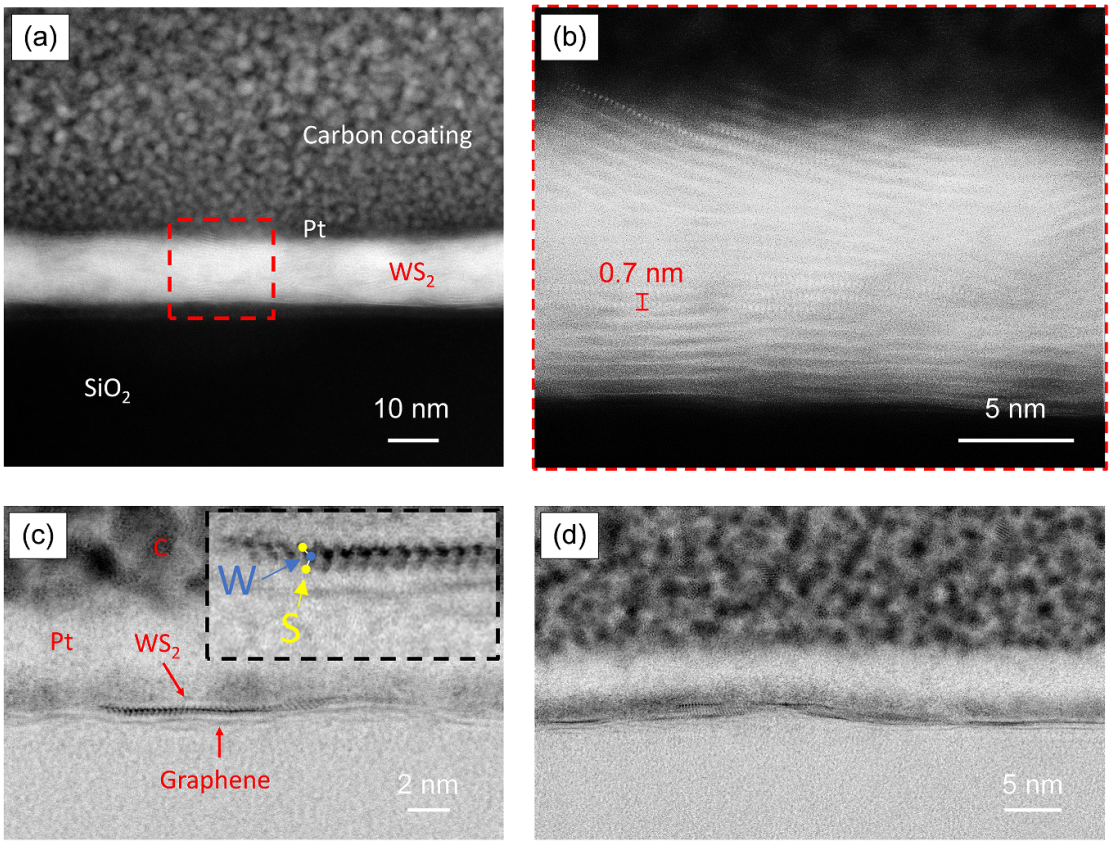

Figure 4. (a) Cross-sectional annular dark-field TEM image of WS_2 electrodeposited for 5 min on patterned graphene electrodes. (b) High magnification image of the highlighted region in (a) showing the layer ordering of the 2D WS_2 growing preferentially in the horizontal direction along the surface of the substrate. (c) and (d) Bright field TEM images of a film grown for 10 s showing regions of electrodeposited films composed of 1–2 layers over graphene.

beam miller. Pt and C were deposited over the film to protect it during the milling process. Figure 4(a) presents an image taken via annular dark field mode showing the WS_2 film in between the SiO_2/Si substrate and the protection layers. A higher magnification image of the highlighted region in (a) is presented in figure 4(b). The image clearly shows the preferential crystallization of the WS_2 layers in the horizontal direction above the substrate. The vertical layer-to-layer distance in the stack was measured to be 0.7 ± 0.1 nm which matches very well with previous work [50]. Overall, it is clear that the film is composed of well-ordered 2D layers and the layer ordering of a particular layer tends to follow that of previous layers. It was noticed that the horizontal layer ordering changes slightly in some regions where the thickness is higher [52]. Figures 4(c) and (d) show high resolution TEM images taken via bright field for a film grown for 10 s. These films are observed to be composed of 1–2 layers only. It is clear to note here the presence of the graphene layer under the WS_2 film which matches TEM images of graphene layers from the literature [53]. The grown WS_2 was also noted to clearly follow the topography of the graphene film. The inset of figure 4(c) show a digital magnification of the atomic structure of the WS_2 film. With a careful look at the inset, the reader should be able to distinguish the W and S atoms in the lattice. We have overlayed a schematic of one molecule to make our indication clearer. The W atoms appears darker in BF compared the S atoms due to their difference in atomic weights.

3.4. XPS

XPS measurements were performed on the electrodeposited WS_2 films to study the effect of annealing the film and to quantify its W:S composition. Figure 5 shows the XPS scans taken at the binding energy ranges of W and S on the as-deposited film (a and b) and after annealing (c and d). A typical W 4f spectrum from WS_2 is composed primarily of a spin doublet corresponding to 4 $f_{5/2}$ and 4 $f_{7/2}$ [54]. Here, these were observed at 32.9 eV and 34.9 eV, respectively. The energy of these peaks corresponds to the 2H phase of WS_2. Another prominent spin doublet (red) was also found at higher energies. The second doublet observed here has been reported by previous studies to be attributed to oxidation, resulting in W^{6+} peaks [55, 56]. These could be related to surface oxidation of the film resulting in the formation of WO_3 [20, 57, 58]. After annealing, the intensity of the W^{6+} peaks reduce significantly and an enhancement in the W^{4+} peaks was observed with a significant reduction in their full width half maximum

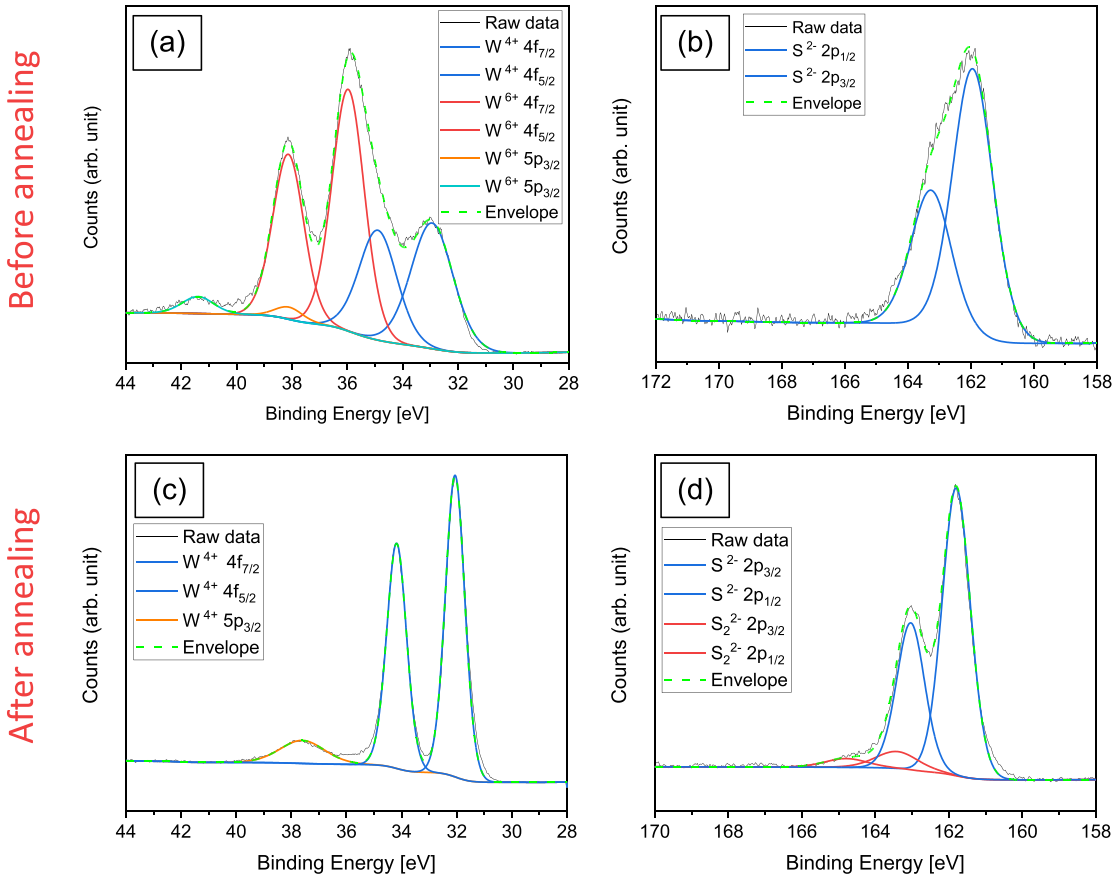

Figure 5. XPS measurements across the W (a) and S (b) binding energy range for the film before and after (c) and (d) annealing. The graphs show clear enhancement in the material crystallinity after annealing as evidenced by the reduction in the FWHM of the emission peaks and the increase in the intensity.

(FWHM). This clearly indicates an enhancement in the crystallinity of the film in the 2H phase. The evolution of the sulfur S 2p (blue) peaks was similar to that of the W^{+4} 4f peaks after annealing. The S $2p_{1/2}$ and $2p_{3/2}$ peaks were measured at 161.9 eV and 163.1 eV, respectively. A clear reduction in the FWHM was also found here, with an increase in the overall intensity of the peaks. A second doublet was also observed (red) which was attributed to S_2^{2-} terminal sulfur bond formation that might have resulted from extra sulfur deposited on the film's surface during the annealing process [59].

4. Conclusions

The electrodeposition of WS_2 over graphene electrodes was demonstrated using a single source precursor. By fabricating graphene micro-electrodes, we were able to demonstrate selective growth of WS_2 films into predefined arbitrary micro-patterns. The electrodeposition of WS_2 was found to be controllable and follows a linear behavior. AFM and Raman spectroscopy confirmed that the electrodeposited materials are highly uniform and of good crystallinity after annealing. High resolution TEM imaging has shown that the films are composed of well-ordered stacks of 2D layers of crystalline WS_2. TEM imaging also confirmed that this method is capable of producing films that are as thin as 1–3 layers. XPS measurements showed the influence of annealing the film on its stoichiometry and crystallinity, aligning with previous studies of WS_2 films grown using other techniques. This work demonstrates the potential of electroplating to enable 2D heterostructures at the microscale using graphene patterned electrodes.

Data availability statement

The data that support the findings of this study are openly available at the following URL/DOI: https://doi.org/10.5258/SOTON/D2045.

Acknowledgments

The research work done in this article was financially supported by the Engineering and Physical Sciences Research Council (EPSRC) through the research Grant EP/P025137/1 (2D layered transition metal dichalcogenide semiconductors via non-aqueous electrodeposition) and the programme Grant EP/N035437/1 (ADEPT—Advanced devices

by electroplating). The authors would like to thank Nikolay Zhelev for technical assistance.

Conflicts of interest

The authors declare no conflicts of interest.

Author contributions

Y J N fabricated the electrodes and performed Raman and X P S characterization; S T performed electrodeposition experiments; S R grew and transferred the graphene electrodes prior to fabrication; V G prepared the precursors and annealed the films, N A and J Z performed A F M microscopy, Y H performed T E M microscopy. C H D G, P N B, G R, N K, R B and A L H supervised the project. Y J N wrote the manuscript with contributions from all authors.

ORCID iDs

Y J Noori https://orcid.org/0000-0001-5285-8779
S Thomas https://orcid.org/0000-0002-7735-788X
S Ramadan https://orcid.org/0000-0002-0013-731X
V K Greenacre https://orcid.org/0000-0002-3381-9616
N M Abdelazim https://orcid.org/0000-0003-2786-3722
Y Han https://orcid.org/0000-0002-7638-6785
R Beanland https://orcid.org/0000-0003-1749-4134
A L Hector https://orcid.org/0000-0002-9964-2163
N Klein https://orcid.org/0000-0001-7854-8592
G Reid https://orcid.org/0000-0001-5349-3468
P N Bartlett https://orcid.org/0000-0002-7300-6900
C H de Groot https://orcid.org/0000-0002-3850-7101

References

[1] Zhao W, Ghorannevis Z, Chu L, Toh M, Kloc C, Tan P-H and Eda G 2013 Evolution of electronic structure in atomically thin sheets of WS_2 and WSe_2 *ACS Nano* **7** 791–7
[2] Zhang Y J, Ideue T, Onga M, Qin F, Suzuki R, Zak A, Tenne R, Smet J H and Iwasa Y 2019 Enhanced intrinsic photovoltaic effect in tungsten disulfide nanotubes *Nature* **570** 349–53
[3] Hu G *et al* 2019 Coherent steering of nonlinear chiral valley photons with a synthetic Au–WS_2 metasurface *Nat. Photonics* **13** 467–72
[4] Yuan L and Huang L 2015 Exciton dynamics and annihilation in WS_2 2D semiconductors *Nanoscale* **7** 7402–8
[5] Peimyoo N, Shang J, Cong C, Shen X, Wu X, Yeow E K L and Yu T 2013 Nonblinking, intense two-dimensional light emitter: monolayer WS_2 triangles *ACS Nano* **7** 10985–94
[6] Barachati F, Fieramosca A, Hafezian S, Gu J, Chakraborty B, Ballarini D, Martinu L, Menon V, Sanvitto D and Kéna-Cohen S 2018 Interacting polariton fluids in a monolayer of tungsten disulfide *Nat. Nanotechnol.* **13** 906–9
[7] Gutiérrez H R, Perea-López N, Elías A L, Berkdemir A, Wang B, Lv R, López-Urías F, Crespi V H, Terrones H and Terrones M 2013 Extraordinary room-temperature photoluminescence in triangular WS_2 monolayers *Nano Lett.* **13** 3447–54
[8] Liu L, Kumar S B, Ouyang Y and Guo J 2011 Performance limits of monolayer transition metal dichalcogenide transistors *IEEE Trans. Electron Devices* **58** 3042–7
[9] Sik Hwang W *et al* 2012 Transistors with chemically synthesized layered semiconductor WS_2 exhibiting 105 room temperature modulation and ambipolar behavior *Appl. Phys. Lett.* **101** 13107
[10] Cho J, Amani M, Lien D-H, Kim H, Yeh M, Wang V, Tan C and Javey A 2020 Centimeter-scale and visible wavelength monolayer light-emitting devices *Adv. Funct. Mater.* **30** 1907941
[11] Zeng L, Tao L, Tang C, Zhou B, Long H, Chai Y, Lau S P and Tsang Y H 2016 High-responsivity UV-vis photodetector based on transferable WS_2 film deposited by magnetron sputtering *Sci. Rep.* **6** 20343
[12] Cao Y *et al* 2017 Optical identification using imperfections in 2D materials *2D Mater.* **4** 045021
[13] Xiao R, Lan C, Li Y, Zeng C, He T, Wang S, Li C, Yin Y and Liu Y 2019 High performance Van der Waals graphene–WS_2–Si heterostructure photodetector *Adv. Mater. Interfaces* **6** 1901304
[14] Lan C, Li C, Wang S, He T, Zhou Z, Wei D, Guo H, Yang H and Liu Y 2017 Highly responsive and broadband photodetectors based on WS_2–graphene van der Waals epitaxial heterostructures *J. Mater. Chem.* C **5** 1494–500
[15] Leng T, Parvez K, Pan K, Ali J, McManus D, Novoselov K S, Casiraghi C and Hu Z 2020 Printed graphene/WS_2 battery-free wireless photosensor on papers *2D Mater.* **7** 24004
[16] Tan H, Fan Y, Zhou Y, Chen Q, Xu W and Warner J H 2016 Ultrathin 2D photodetectors utilizing chemical vapor deposition grown WS_2 with graphene electrodes *ACS Nano* **10** 7866–73
[17] Kim B H, Gu H H and Yoon Y J 2018 Large-area and low-temperature synthesis of few-layered WS 2 films for photodetectors *2D Mater.* **5** 45030
[18] Balasubramanyam S, Merkx M J M, Verheijen M A, Kessels W M M, Mackus A J M and Bol A A 2020 Area-selective atomic layer deposition of two-dimensional WS_2 nanolayers *ACS Mater. Lett.* **2** 511–8
[19] Tian K, Baskaran K and Tiwari A 2018 Growth of two-dimensional WS_2 thin films by pulsed laser deposition technique *Thin Solid Films* **668** 69–73
[20] Abbas O A *et al* 2020 Solution-based synthesis of few-layer WS_2 large area continuous films for electronic applications *Sci. Rep.* **10** 1696
[21] Jha R K and Guha P K 2016 Liquid exfoliated pristine WS_2 nanosheets for ultrasensitive and highly stable chemiresistive humidity sensors *Nanotechnology* **27** 475503
[22] Thomas S, Greenacre V K, Smith D E, Noori Y J, Abdelazim N, Hector A L, de Groot C, Levason W, Bartlett P N and Reid G 2021 Tungsten disulfide thin films via electrodeposition from a single source precursor *Chem. Commun.* **57** 10194–7
[23] Kim M, Seo J, Kim J, Moon J S, Lee J, Kim J-H, Kang J and Park H 2021 High-crystalline monolayer transition metal dichalcogenides films for wafer-scale electronics *ACS Nano* **15** 3038–46
[24] Tan H, Xu W, Sheng Y, Lau C S, Fan Y, Chen Q, Tweedie M, Wang X, Zhou Y and Warner J H 2017 Lateral graphene-contacted vertically stacked WS_2/MoS_2 hybrid photodetectors with large gain *Adv. Mater.* **29** 1702917
[25] Zhou X and Yu G 2021 Preparation engineering of two-dimensional heterostructures via bottom-up growth for device applications *ACS Nano* **15** 11040–65
[26] Ni Z H, Wang H M, Luo Z Q, Wang Y Y, Yu T, Wu Y H and Shen Z X 2010 The effect of vacuum annealing on graphene *J. Raman Spectrosc.* **41** 479–83

[27] Khadka S, Lindquist M, Aleithan S H, Blumer A N, Wickramasinghe T E, Kordesch M E and Stinaff E 2017 Concurrent growth and formation of electrically contacted monolayer transition metal dichalcogenides on bulk metallic patterns *Adv. Mater. Interfaces* **4** 1600599
[28] Ahlberg P, Johansson F O L, Zhang Z-B, Jansson U, Zhang S-L, Lindblad A and Nyberg T 2016 Defect formation in graphene during low-energy ion bombardment *APL Mater.* **4** 46104
[29] Maneshian M H, Kuo F-L, Mahdak K, Hwang J, Banerjee R and Shepherd N D 2011 The influence of high dielectric constant aluminum oxide sputter deposition on the structure and properties of multilayer epitaxial graphene *Nanotechnology* **22** 205703
[30] Osaka T 2000 Electrodeposition of highly functional thin films for magnetic recording devices of the next century *Electrochim. Acta* **45** 3311–21
[31] Kondo K, Yamakawa N, Tanaka Z and Hayashi K 2003 Copper damascene electrodeposition and additives *J. Electroanal. Chem.* **559** 137–42
[32] Noori Y J *et al* 2020 Large-area electrodeposition of few-layer MoS_2 on graphene for 2D material heterostructures *ACS Appl. Mater. Interfaces* **12** 49786–94
[33] Thomas S, Smith D E, Greenacre V K, Noori Y J, Hector A L, de Groot C K, Reid G and Bartlett P N 2020 Electrodeposition of MoS_2 from dichloromethane *J. Electrochem. Soc.* **167** 106511
[34] Pu Z, Liu Q, Asiri A M, Obaid A Y and Sun X 2014 One-step electrodeposition fabrication of graphene film-confined WS_2 nanoparticles with enhanced electrochemical catalytic activity for hydrogen evolution *Electrochim. Acta* **134** 8–12
[35] Fan L and Suni I I 2017 Electrodeposition and capacitance measurements of WS_2 thin films *J. Electrochem. Soc.* **164** D681–6
[36] Devadasan J J, Sanjeeviraja C and Jayachandran M 2001 Electrodeposition of p-WS_2 thin film and characterisation *J. Cryst. Growth* **226** 67–72
[37] Huang R *et al* 2019 Towards a 3D GeSbTe phase change memory with integrated selector by non-aqueous electrodeposition *Faraday Discuss.* **213** 339–55
[38] Noori Y J *et al* 2021 Phase-change memory by GeSbTe electrodeposition in crossbar arrays *ACS Appl. Electron. Mater.* **3** 3610–8
[39] Lee Y, Bae S, Jang H, Jang S, Zhu S-E, Sim S H, Song Y Il, Hong B H and Ahn J-H 2010 Wafer-scale synthesis and transfer of graphene films *Nano Lett.* **10** 490–3
[40] Lee J-H *et al* 2014 Wafer-scale growth of single-crystal monolayer graphene on reusable hydrogen-terminated germanium *Science* **344** 286 LP—289
[41] Whelan P R *et al* 2021 Case studies of electrical characterisation of graphene by terahertz time-domain spectroscopy *2D Mater.* **8** 022003
[42] Tsang D K H, Lieberthal T J, Watts C, Dunlop I E, Ramadan S, Del Rio Hernandez A E and Klein N 2019 Chemically functionalised graphene FET biosensor for the label-free sensing of exosomes *Sci. Rep.* **9** 13946
[43] Ramadan S *et al* 2021 Carbon-dot-enhanced graphene field-effect transistors for ultrasensitive detection of exosomes *ACS Appl. Mater. Interfaces* **13** 7854–64
[44] Ferrari A C *et al* 2006 Raman spectrum of graphene and graphene layers *Phys. Rev. Lett.* **97** 187401
[45] Liu -W-W, Chai S-P, Mohamed A R and Hashim U 2014 Synthesis and characterization of graphene and carbon nanotubes: a review on the past and recent developments *J. Ind. Eng. Chem.* **20** 1171–85
[46] Sahoo S, Palai R and Katiyar R S 2011 Polarized Raman scattering in monolayer, bilayer, and suspended bilayer graphene *J. Appl. Phys.* **110** 044320
[47] Wang Y Y, Gao R X, Ni Z H, He H, Guo S P, Yang H P, Cong C X and Yu T 2012 Thickness identification of two-dimensional materials by optical imaging *Nanotechnology* **23** 495713
[48] Li H, Wu J, Huang X, Lu G, Yang J, Lu X, Xiong Q and Zhang H 2013 Rapid and reliable thickness identification of two-dimensional nanosheets using optical microscopy *ACS Nano* **7** 10344–53
[49] Greenacre V K, Hector A L, Levason W, Reid G, Smith D E and Sutcliffe L 2019 Complexes of $WOCl_4$ and $WSCl_4$ with neutral N- and O-donor ligands: synthesis, spectroscopy and structures *Polyhedron* **162** 14–19
[50] Berkdemir A *et al* 2013 Identification of individual and few layers of WS_2 using Raman spectroscopy *Sci. Rep.* **3** 1755
[51] Peimyoo N, Shang J, Yang W, Wang Y, Cong C and Yu T 2015 Thermal conductivity determination of suspended mono- and bilayer WS_2 by Raman spectroscopy *Nano Res.* **8** 1210–21
[52] Abdelazim N M *et al* 2021 Lateral growth of MoS_2 2D material semiconductors over an insulator via electrodeposition *Adv. Electron. Mater.* **7** 2100419
[53] Norimatsu W and Kusunoki M 2014 Epitaxial graphene on SiC{0001}: advances and perspectives *Phys. Chem. Chem. Phys.* **16** 3501–11
[54] Sang Y, Zhao Z, Zhao M, Hao P, Leng Y and Liu H 2015 From UV to near-infrared, WS_2 nanosheet: a novel photocatalyst for full solar light spectrum photodegradation *Adv. Mater.* **27** 363–9
[55] Liu W, Benson J, Dawson C, Strudwick A, Raju A P A, Han Y, Li M and Papakonstantinou P 2017 The effects of exfoliation, organic solvents and anodic activation on the catalytic hydrogen evolution reaction of tungsten disulfide *Nanoscale* **9** 13515–26
[56] Tan S M and Pumera M 2016 Bottom-up electrosynthesis of highly active tungsten sulfide (WS_{3-x}) films for hydrogen evolution *ACS Appl. Mater. Interfaces* **8** 3948–57
[57] Alsabban M M, Min S, Hedhili M N, Ming J, Li L-J and Huang K-W 2016 Editors' choice—growth of layered WS_2 electrocatalysts for highly efficient hydrogen production reaction *ECS J. Solid State Sci. Technol.* **5** Q3067–71
[58] Martin-Litas I, Vinatier P, Levasseur A, Dupin J C, Gonbeau D and Weill F 2002 Characterisation of r.f. sputtered tungsten disulfide and oxysulfide thin films *Thin Solid Films* **416** 1–9
[59] Huang G, Liu H, Wang S, Yang X, Liu B, Chen H and Xu M 2015 Hierarchical architecture of WS_2 nanosheets on graphene frameworks with enhanced electrochemical properties for lithium storage and hydrogen evolution *J. Mater. Chem.* A **3** 24128–38